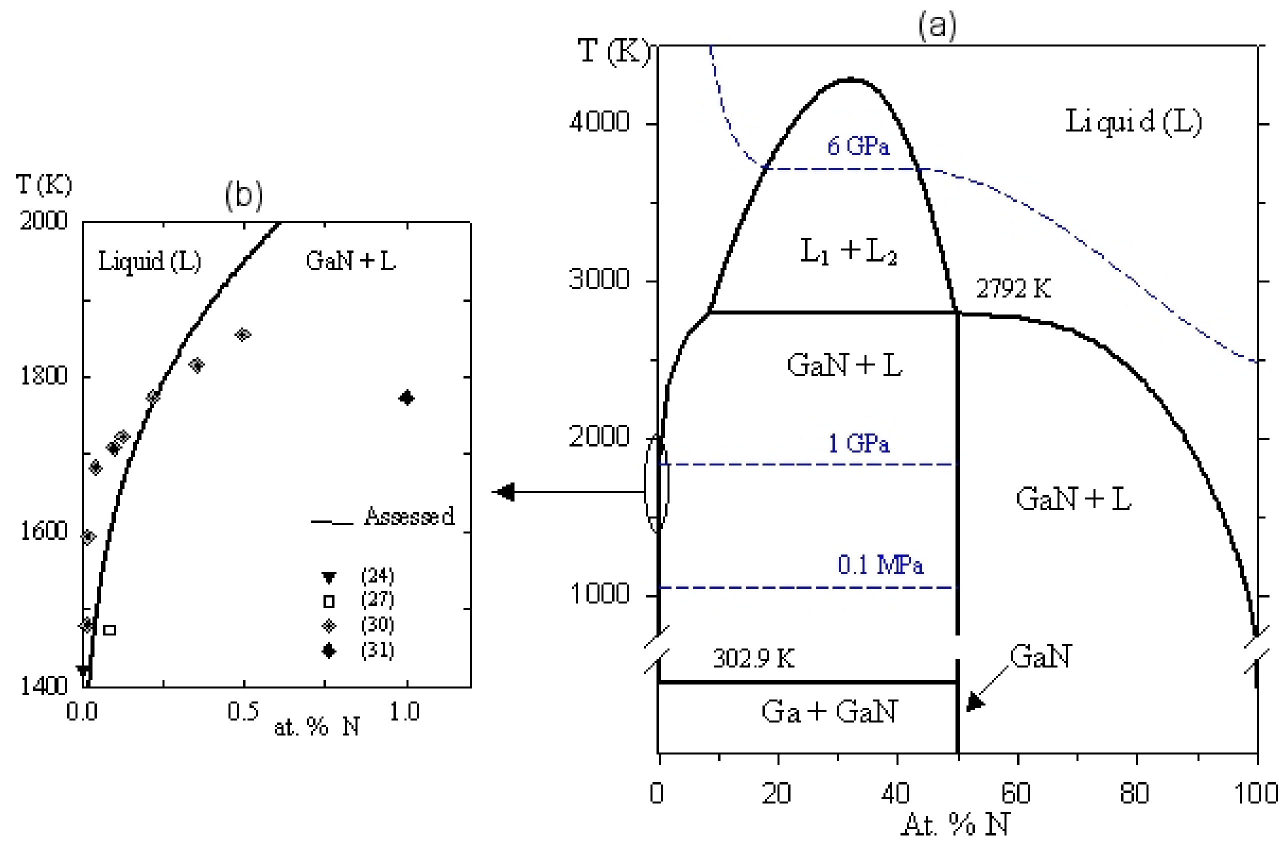

Figure 2-1 The calculated binary phase diagram of GaN

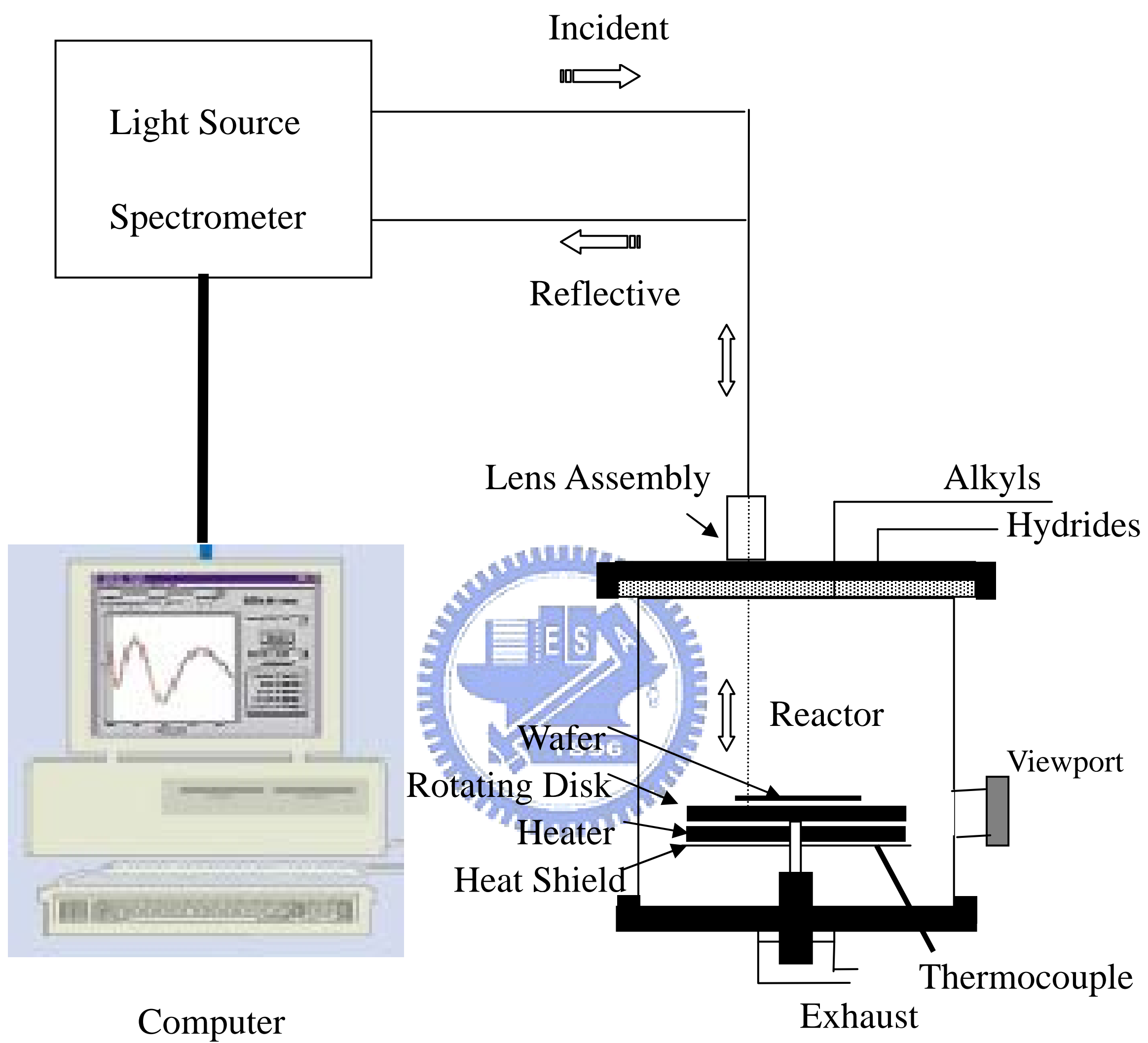

Figure 2-2. Schematic diagram of the in-situ monitoring system.

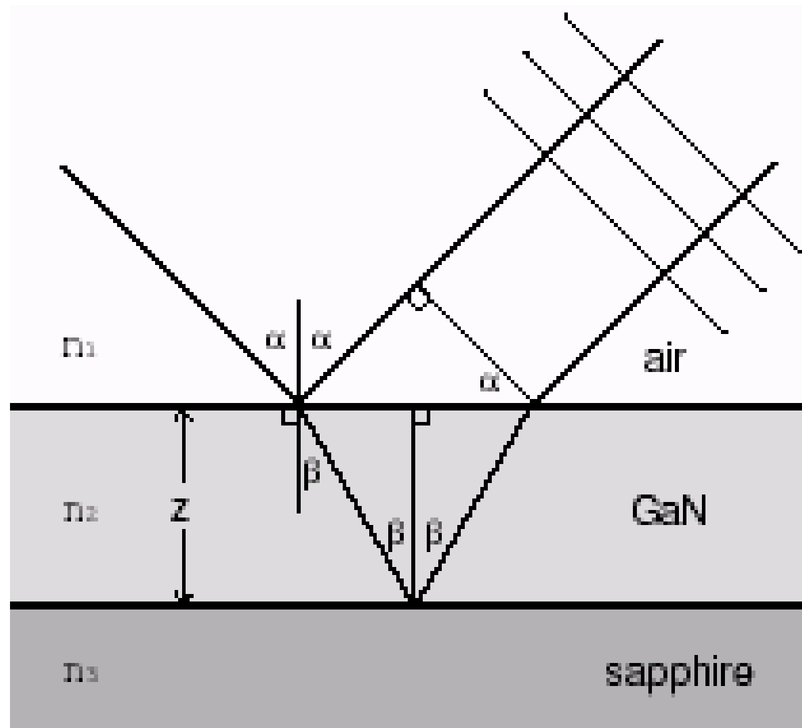

(a)

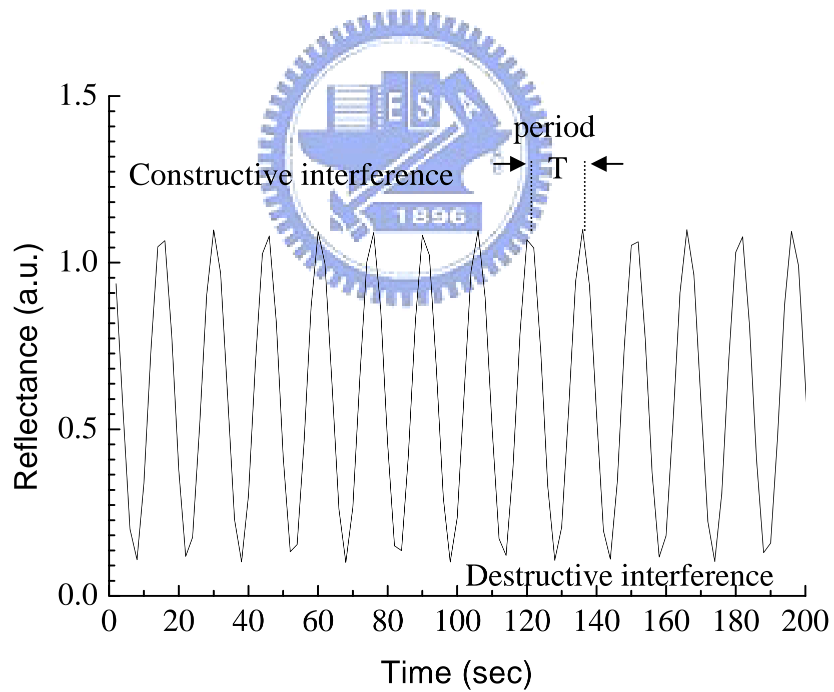

(b)

Figure 2-3. (a) A diagram of thin-film interference with dielectric materials. Coherent light illuminates the wafer surface during the film deposition and the reflected light is sampled with a photodiode. (b) The reflectance spectrum for single layer epitaxy in constant growth rate case.

(a). Pretreatment of sapphire substrate

(b). buffer GaN growth

(c). epitaxy GaN growth

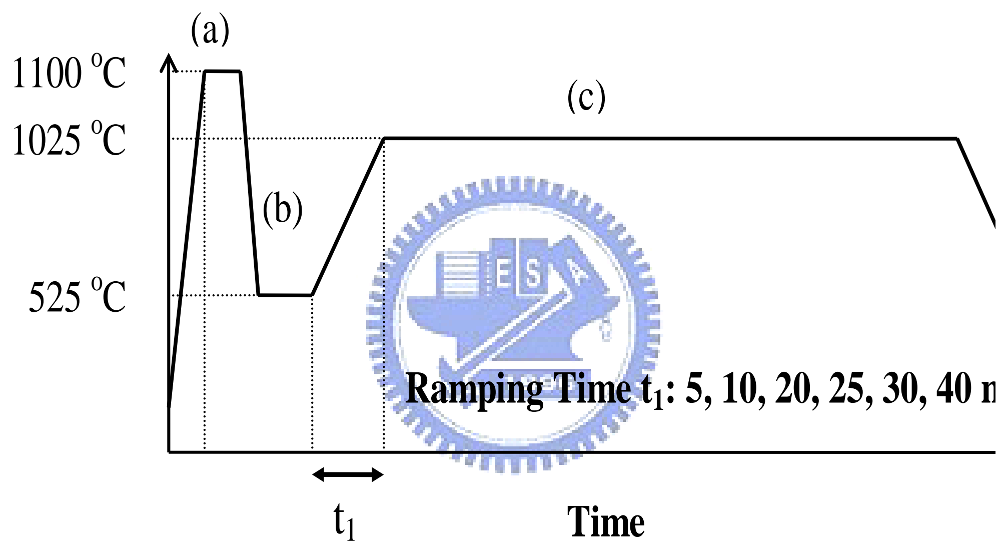

Figure 2-4 Thermal profile for the growth of GaN epitaxial layer. The ramping time t_1 varied from 525℃ to 1025℃ after the grown LT-GaN buffer layer.

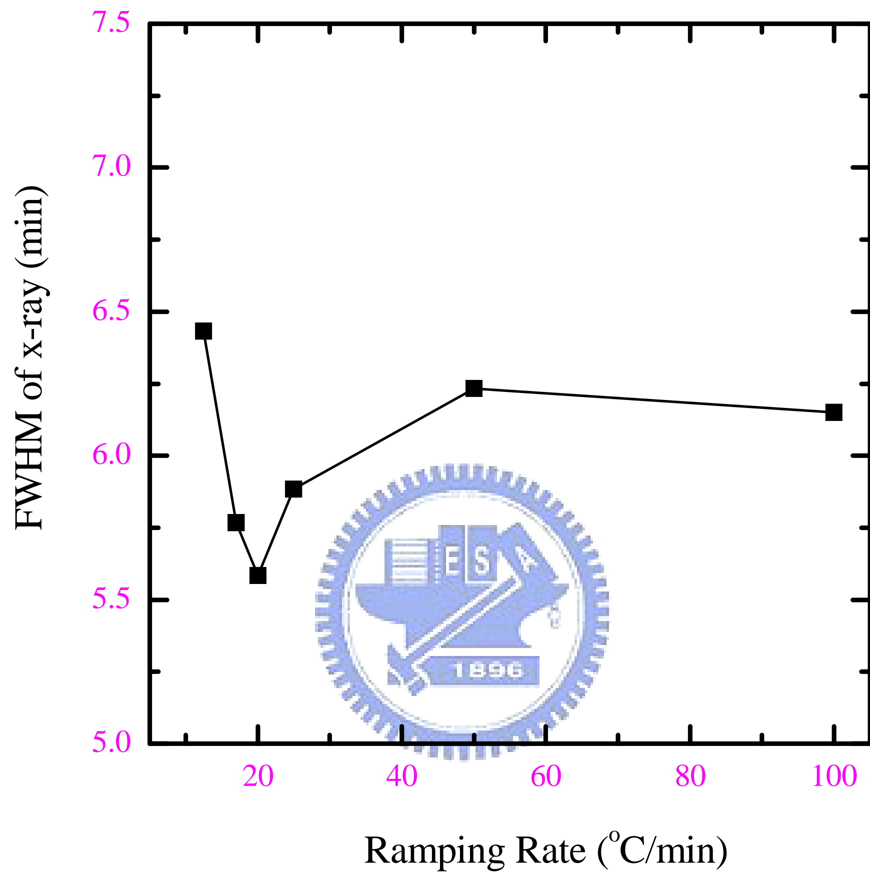

Figure 2-5. The FWHM of XRD for (0004) diffraction from the GaN epitaxial layer as a function of the temperature ramping rate between 525℃ and 1025℃ after grown LT-GaN buffer layer

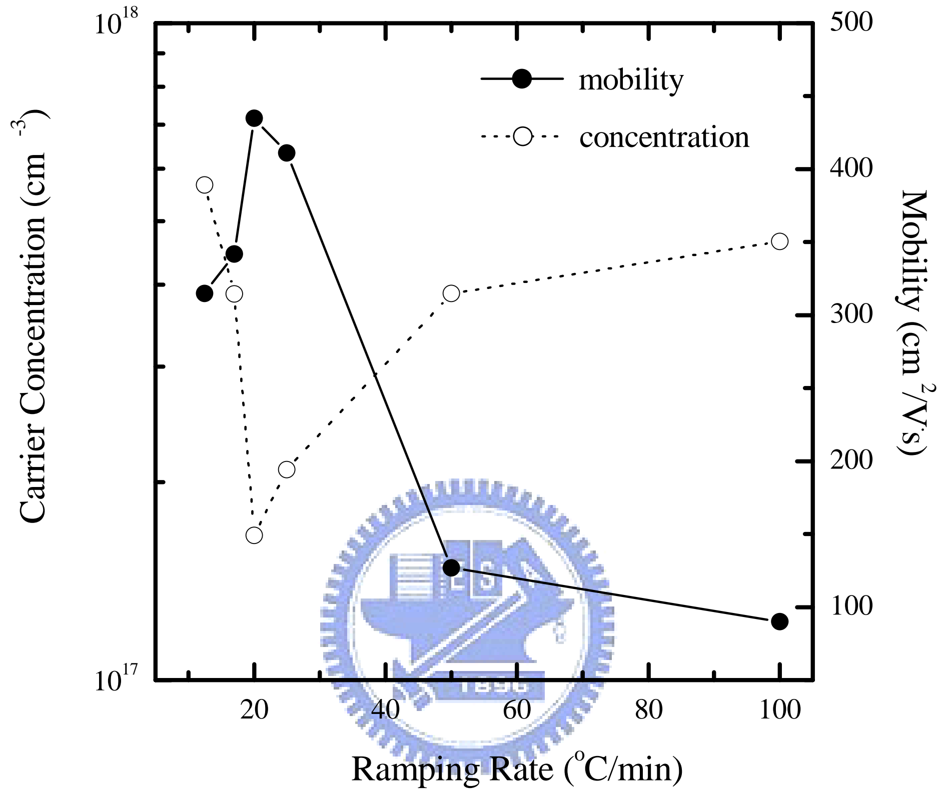

Figure 2-6. The Hall mobility and carrier concentration measured at 300K as a function of the temperature ramping rate between 525℃ and 1025℃ after grown LT-GaN buffer layer.

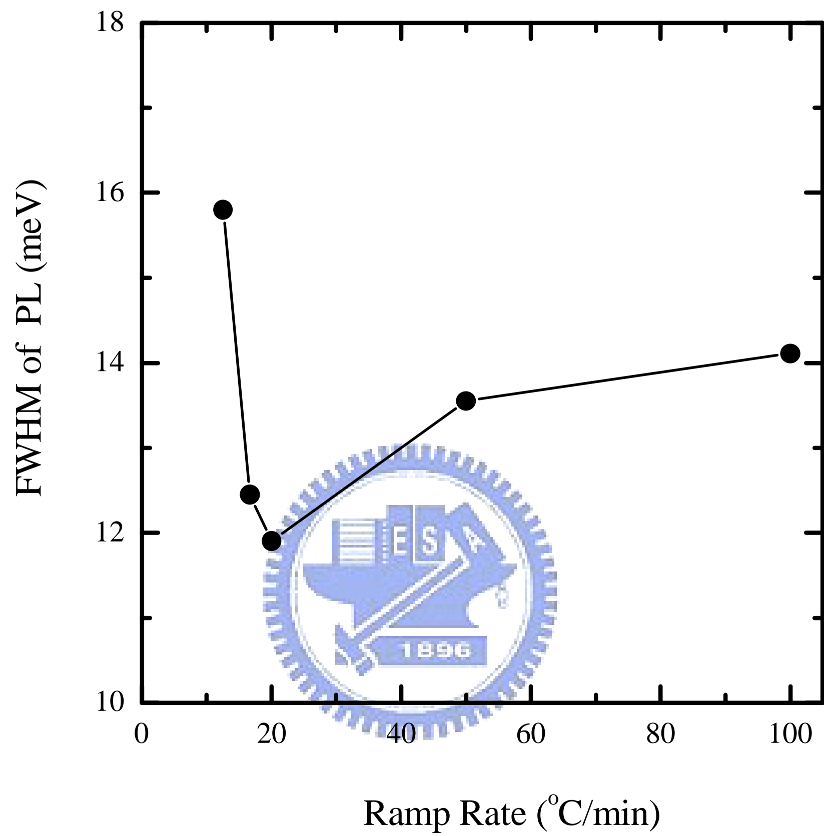

Figure 2-7. 10K photoluminescence linewidths (FWHM) for GaN epitaxial layer as a function of the temperature ramping rate between 525℃ and 1025℃ after grown LT-GaN buffer layer.

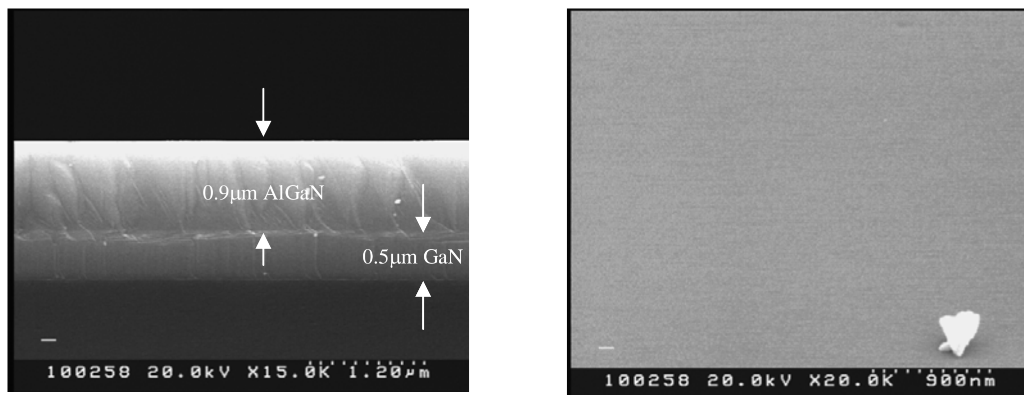

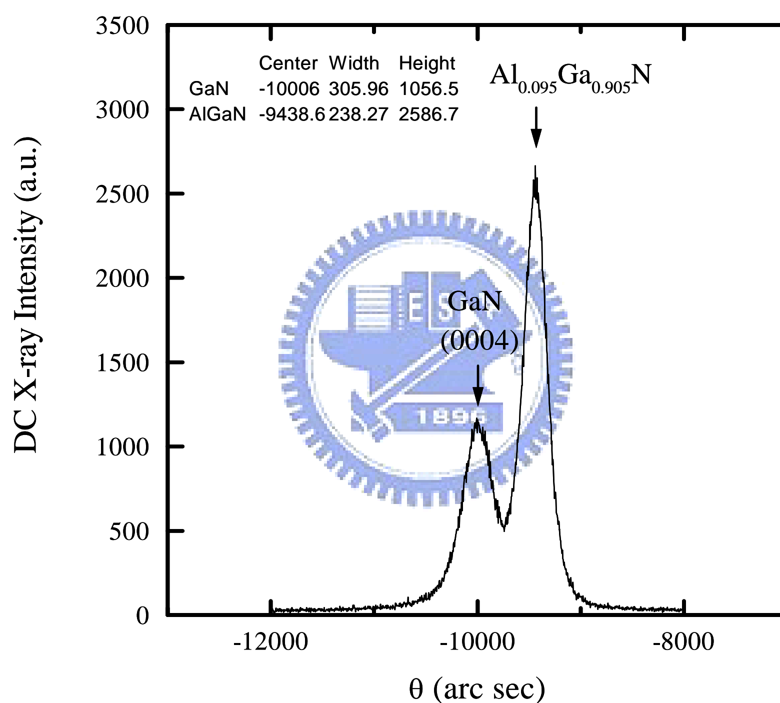

Figure 2-8. The thickness and surface morphology of AlGaN/GaN double layers were observed from the SEM photograph. The GaN (0004) and $Al_xGa_{1-x}N$ (0004) peaks were showed in x-ray diffraction curve.

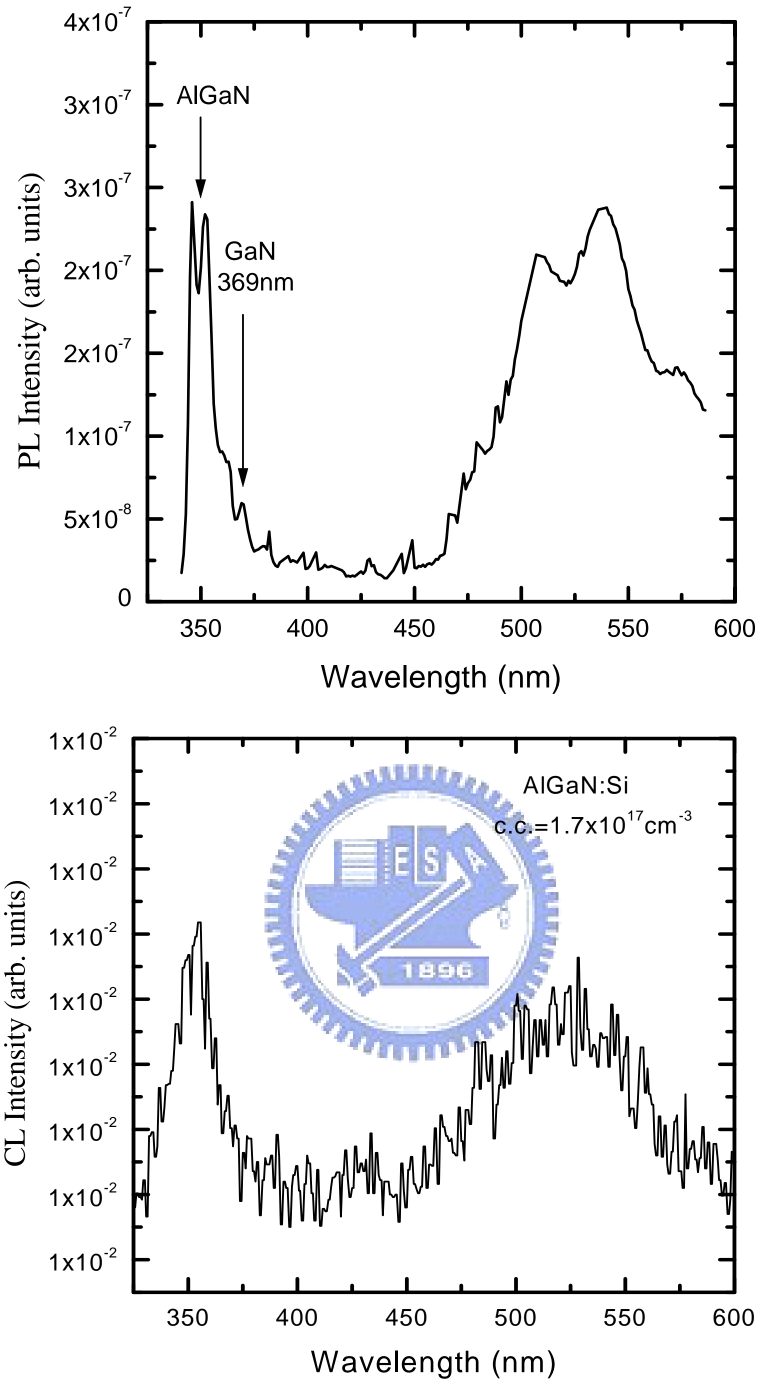

Figure 2-9. The AlGaN peak, GaN peak and yellow peak were observed from PL and CL Spectrums at RT

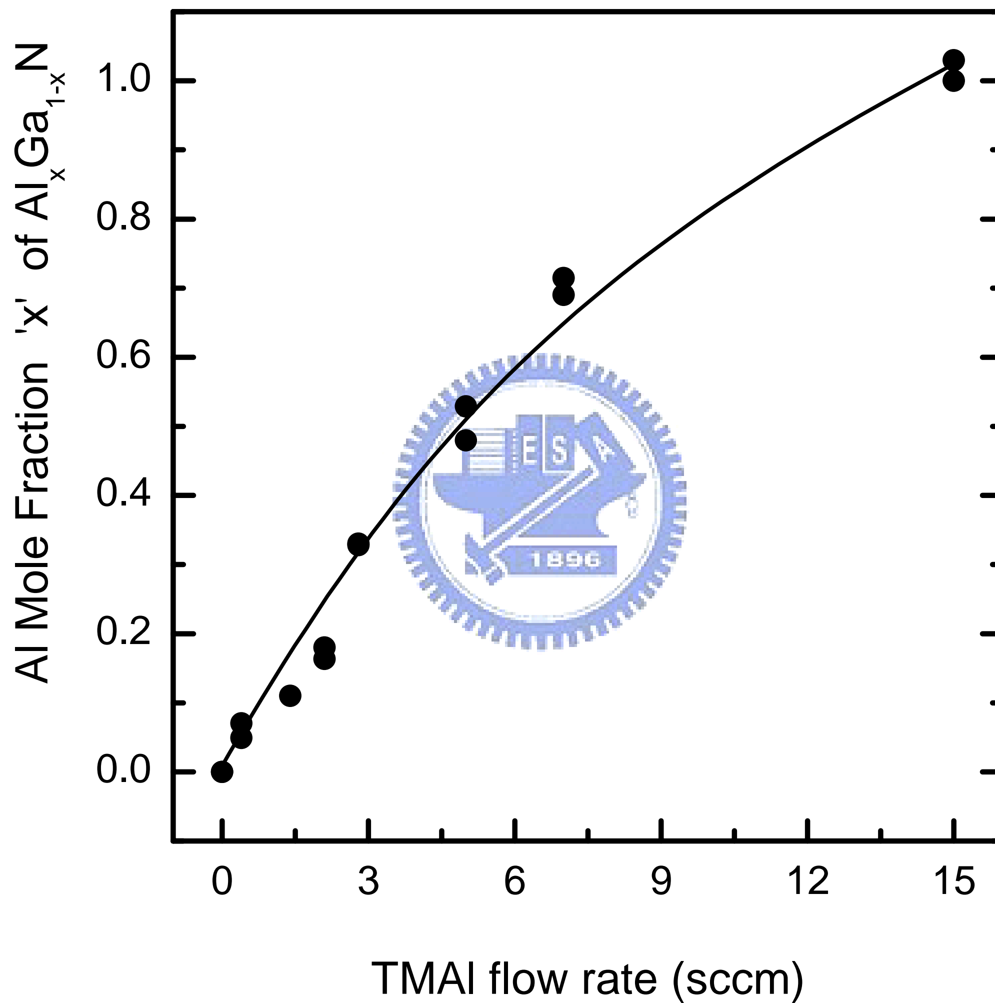

Figure 2-10. The dependence of Al mole fraction on TMAl flow rate for $A_xlGa_{1-x}N$ epitaxial growth.

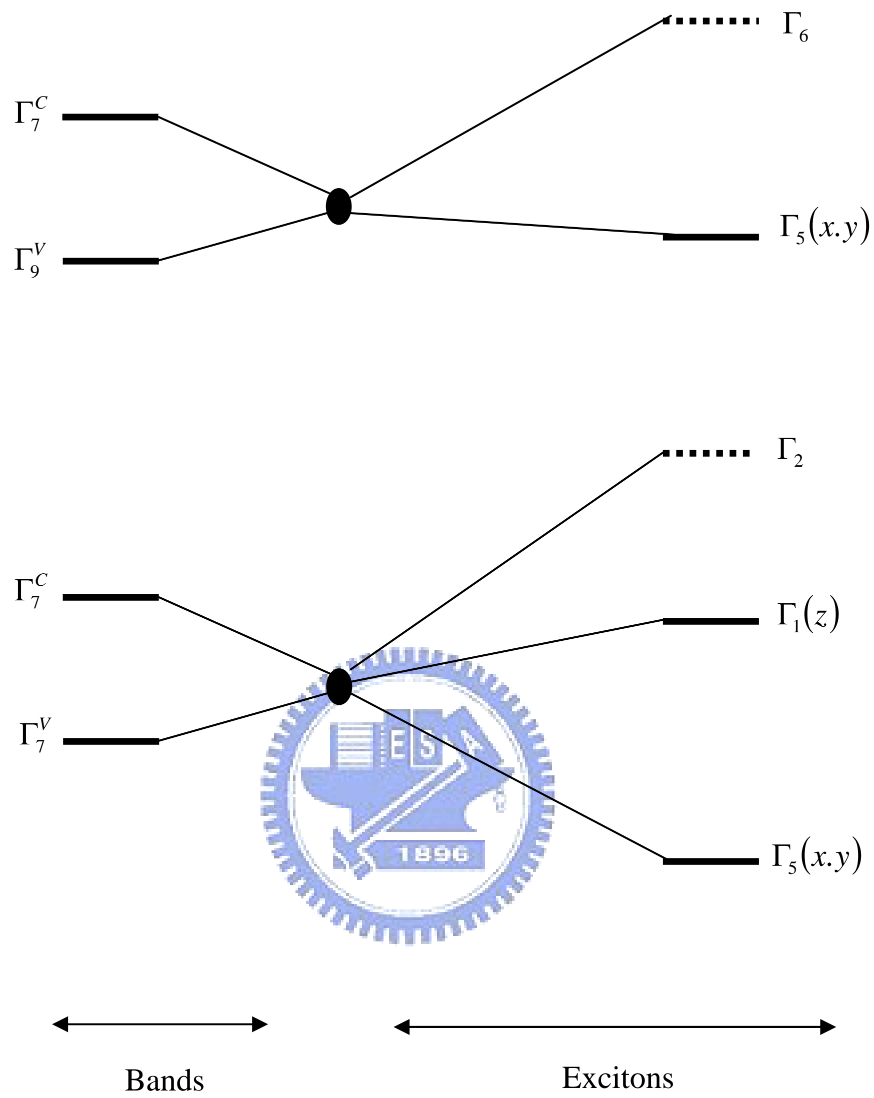

Figure 2-11. Sketch of the construction of the exciton states from the combination of conduction and valence band Bloch state for epitaxy on C-plane.

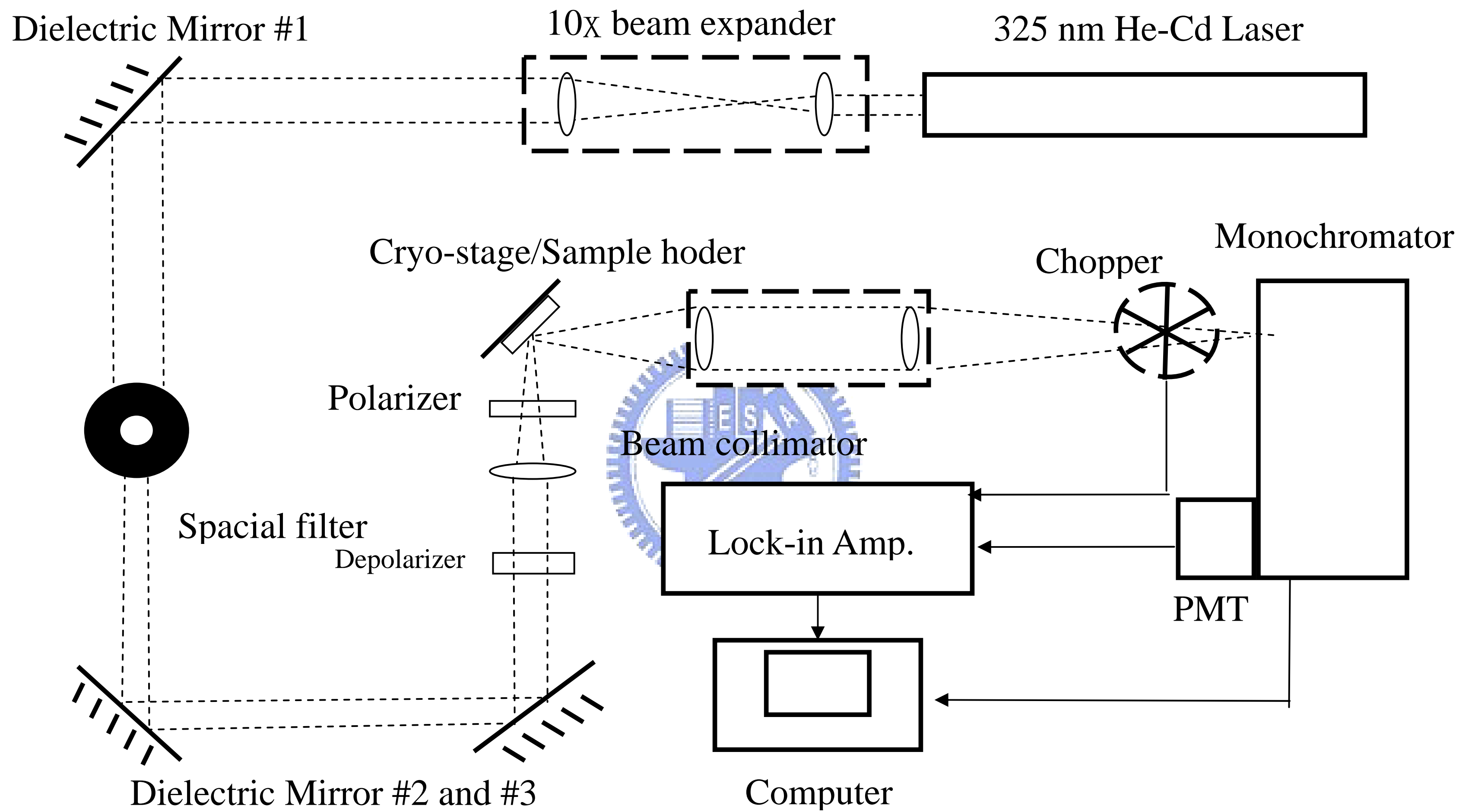

Figure 2-12. Schematic of PL measurement system.

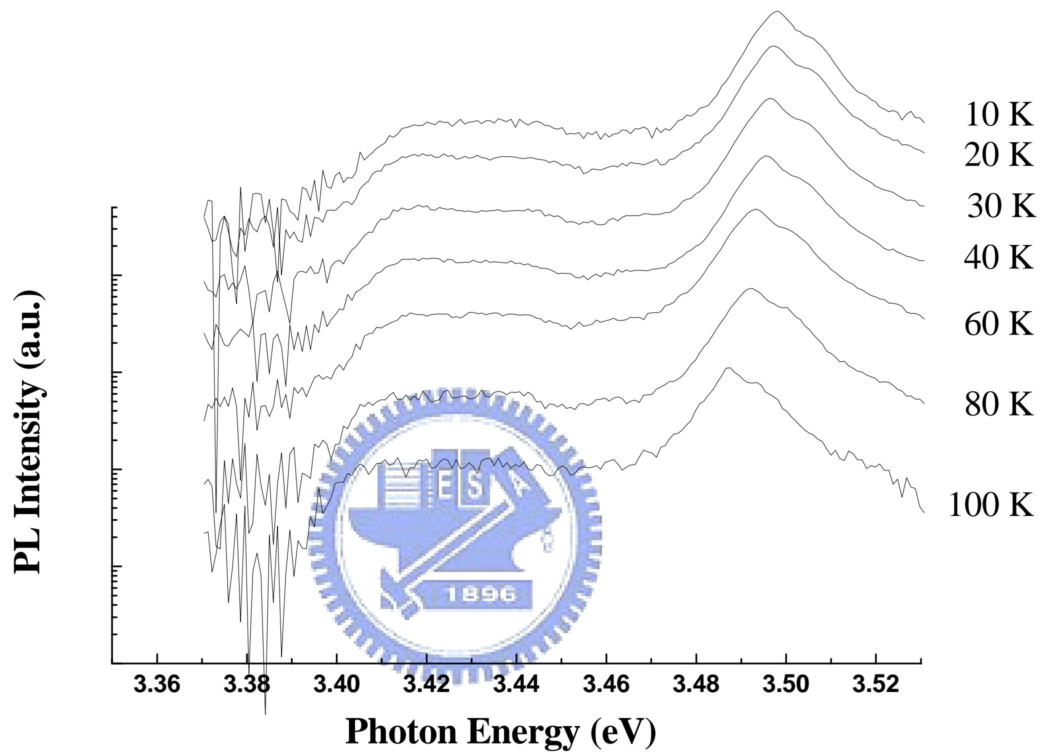

Figure 2-13. Typical PL spectra near the band edge emissions at low temperatures.

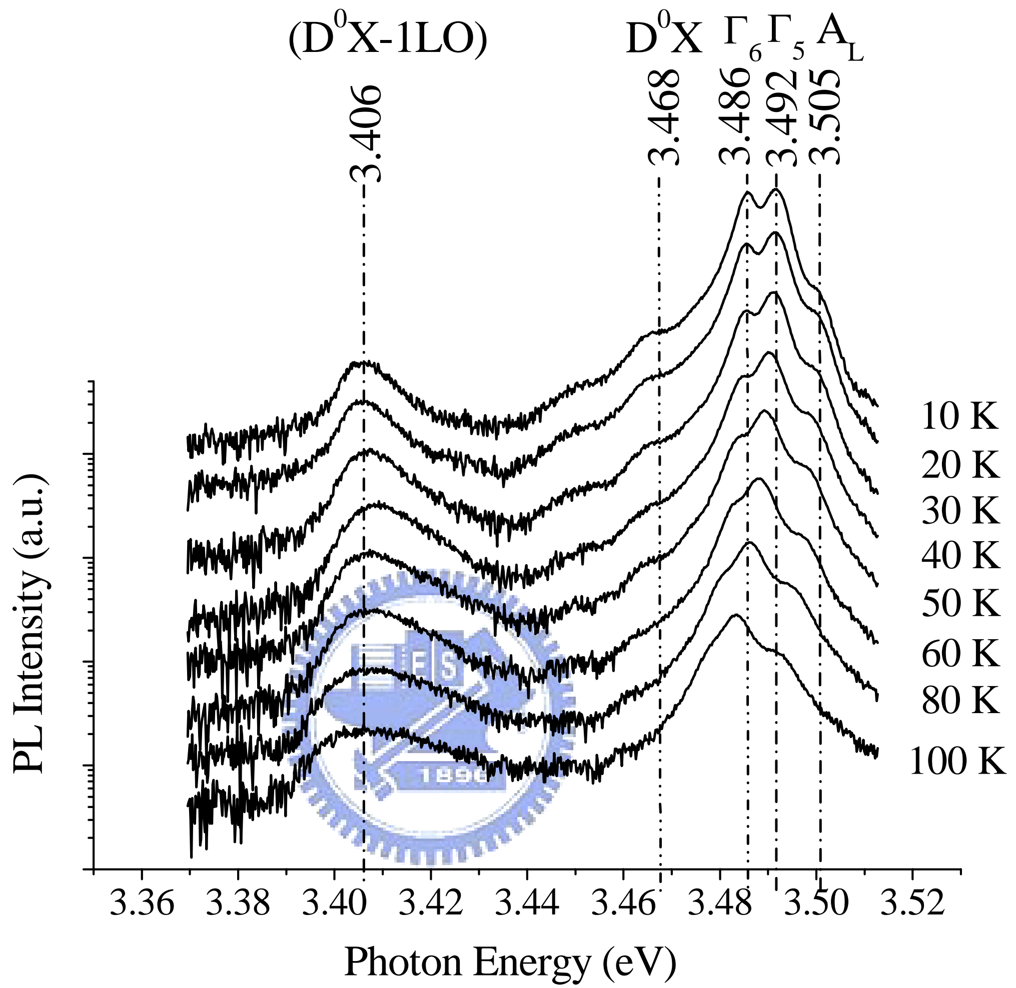

Figure 2-14. PL spectra of the high quality UID GaN at different temperature.

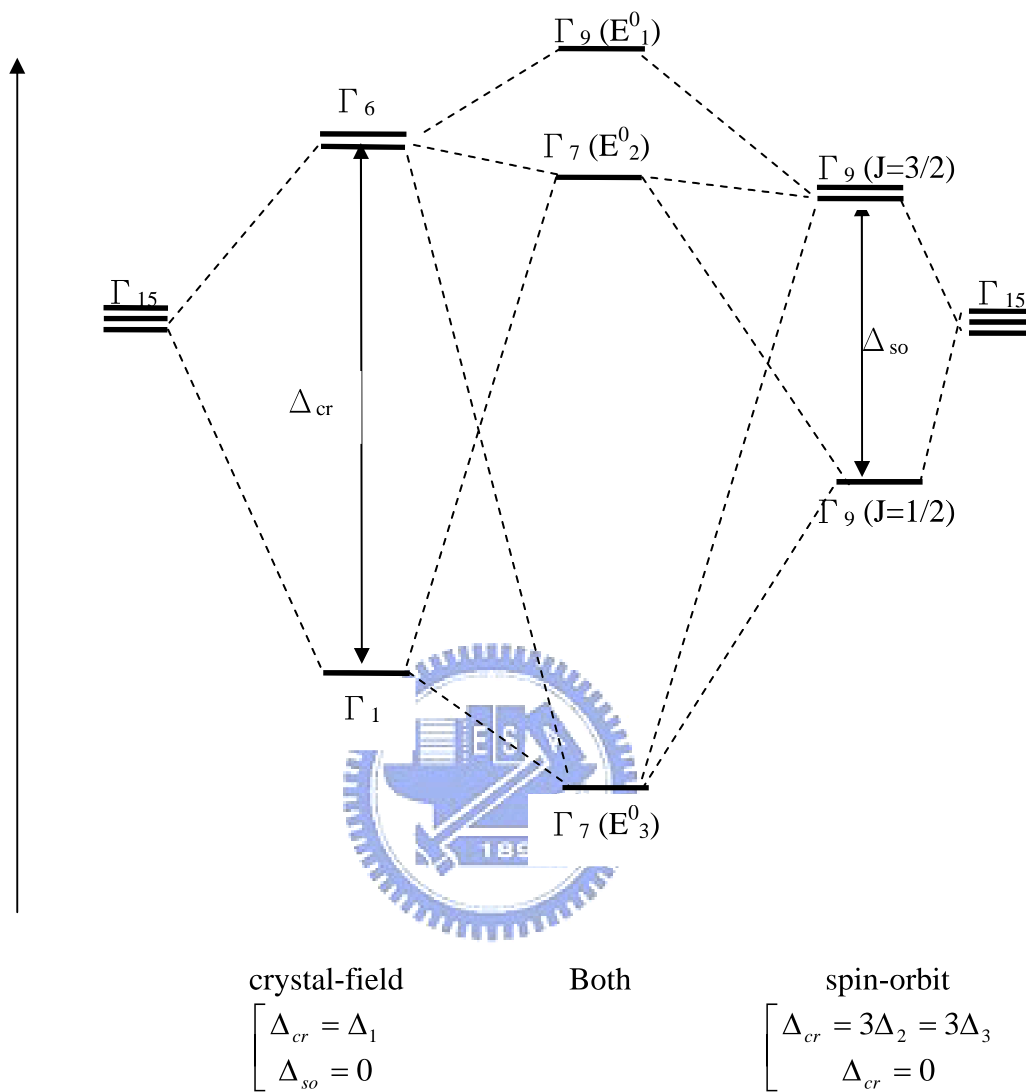

$$\begin{cases} \Delta_{cr} = \Delta_1 \\ \Delta_{so} = 0 \end{cases} \qquad \begin{cases} \Delta_{cr} = 3\Delta_2 = 3\Delta_3 \\ \Delta_{cr} = 0 \end{cases}$$

Figure 2-15. Energy splitting at the top of the valence bands of GaN under the influence of crystal-field and spin-orbit coupling. (The figure is not drawn to scale.)

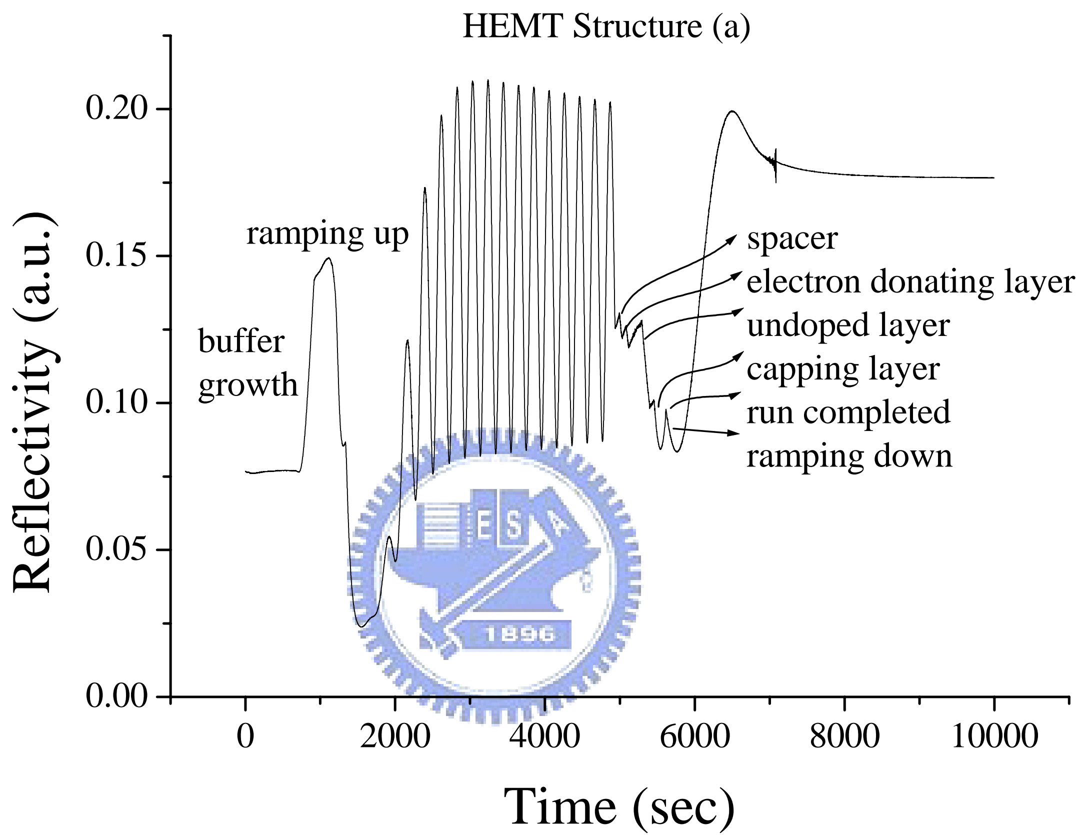

Figure 2-16. Typical reflection spectrum of U-GaN and AlGaN/GaN HEMT.

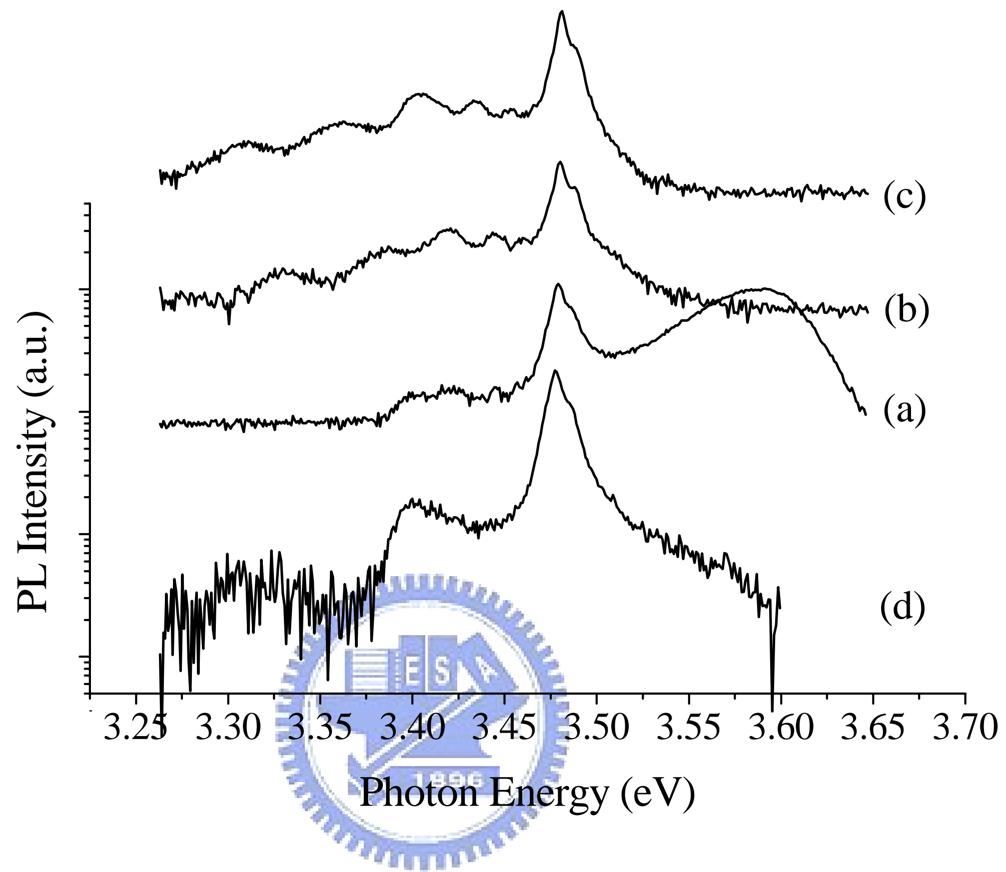

Figure 2-17. PL Spectra at 10 K for different structures of $Al_{0.06}Ga_{0.94}N$ / $Al_xGa_{1-x}N$ / δ -doping /$Al_{0.15}G_{0.85}N$ / GaN HEMTs.

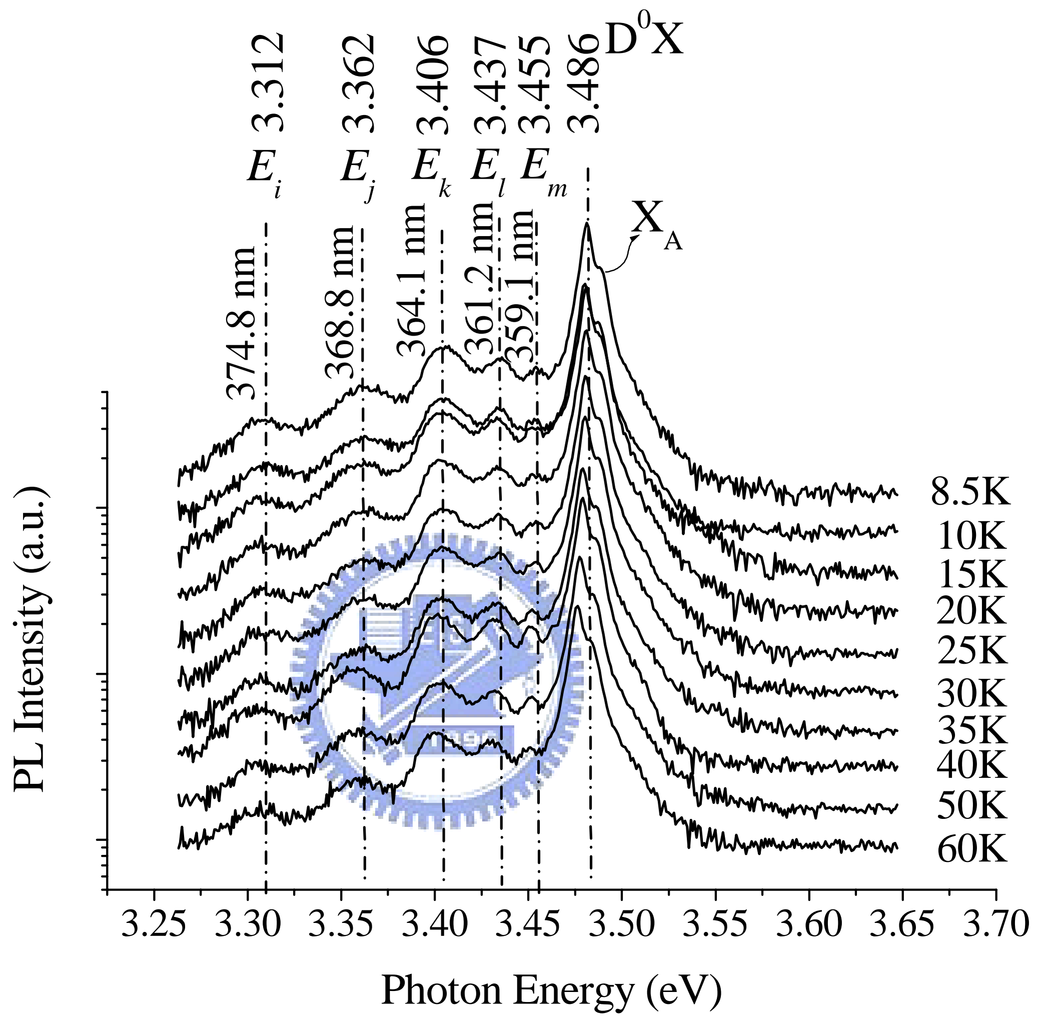

Figure 2-18. Temperature dependent PL spectra for the sample (c). Notice that the peak red-shift of the GaN D^{0}X is larger than that in 2-DEG.

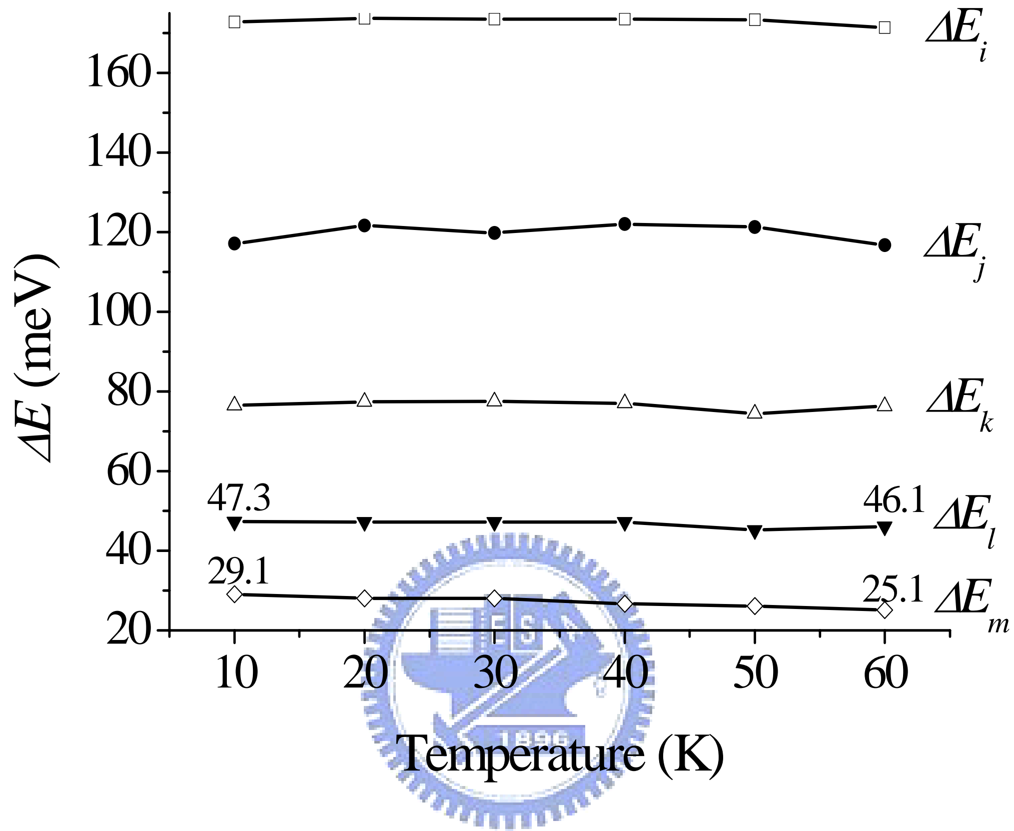

Figure 2-19. Temperature dependence of the energy separation (△E) of the 2DEG subbands PL peak form the GaN D^0X emission where $\Delta E_i = E_{D^0X} - E_i$ and so on.

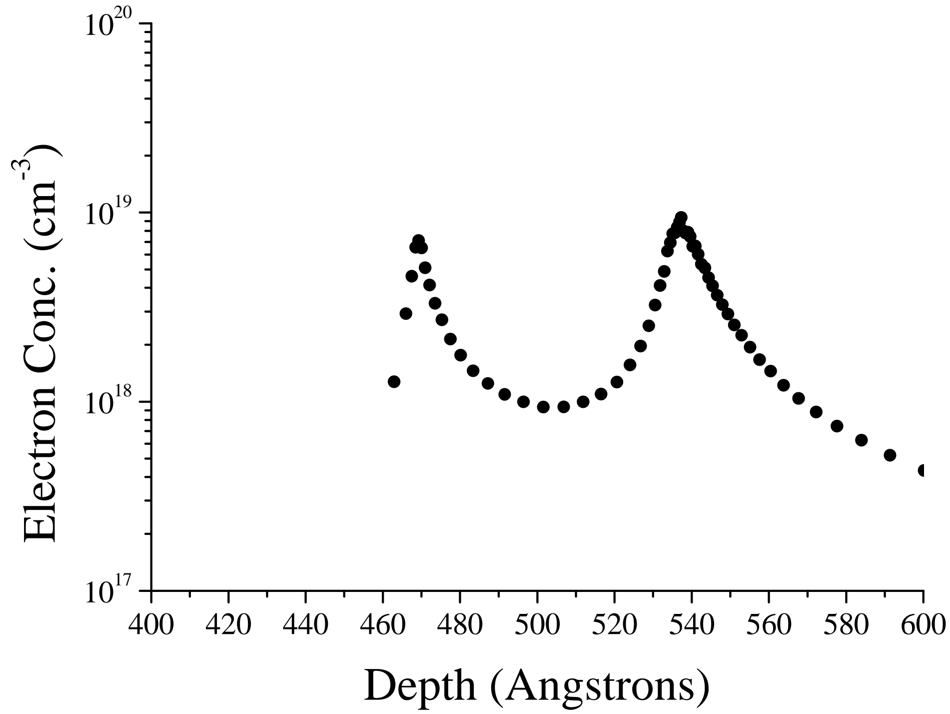

(a)

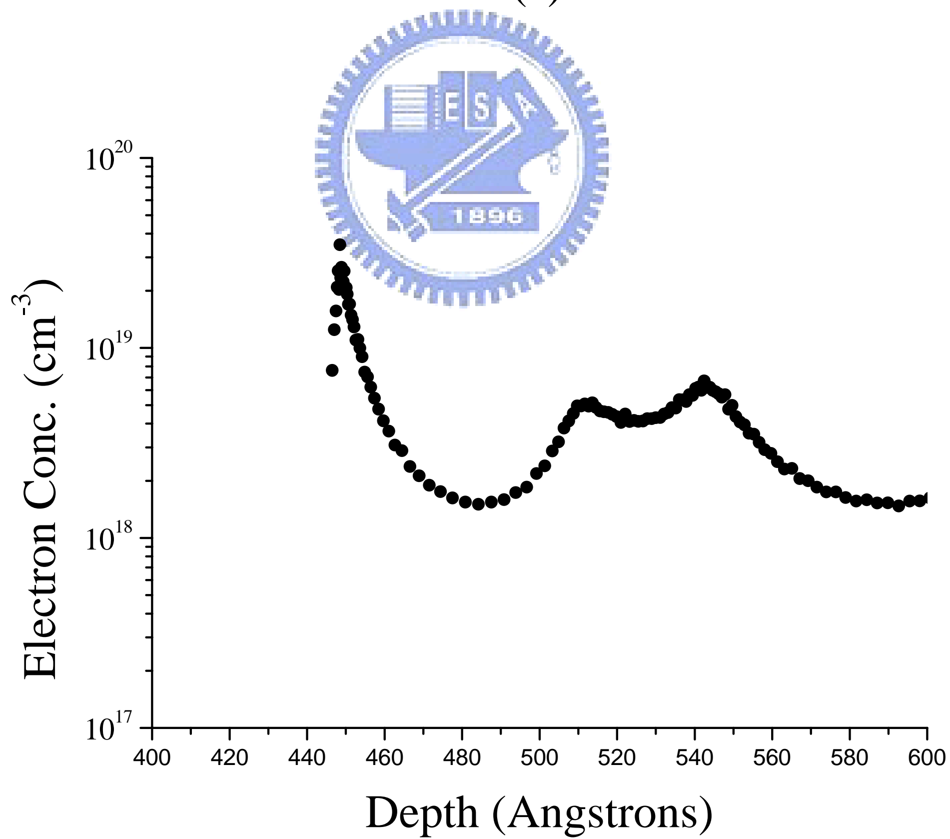

(b)

Figure 2-20. The CV plots of HEMT for (a) sample-c and (b) sample-d.